Geomorphology 230 (2015) 161–170

Contents lists available at ScienceDirect

Geomorphology

journal homepage: www.elsevier.com/locate/geomorph

Unravelling the multiphase run-out conditions of a slide-flow mass movement

Th.W.J. van Asch [a,b,*], Q. Xu [b], X.J. Dong [b]

[a] Faculty of Geosciences,Utrecht University, P.O. Box 80115, 3508 TC, Utrecht, The Netherlands
[b] State Key Laboratory of Geohazards Prevention and Environment Protection, University of Technology, No. 1 Erxianqiao East Rd., Chengdu, Sichuan 610059, China

ARTICLE INFO

Article history:
Received 15 March 2014
Received in revised form 9 November 2014
Accepted 24 November 2014
Available online 28 November 2014

Keywords:
Rock slide
Debris flow
Two-phase run-out modelling
Entrainment
Deposition geometry
Changing rheologies

ABSTRACT

In this paper an attempt is made to unravel the run-out characteristics of a mass movement in the Sichuan Province, SW China by means of 1D numerical modelling and calibration on the topography of run-out profiles. The Dagou mass movement started as a rockslide with an initial volume of 480,000 m^3, which transformed into a debris flow, increasing in volume due to entrainment of loose material in the upper part of the travelling track. The rapid mass movement had a run-out distance of 1380 m and a run-out time of about 50 s.

Numerical calculations were conducted with the depth average shallow water equation to explain the variation in thickness of the debris flow deposits along the run-out track. For the calibration of the first run-out phase, three rheological models were applied, namely the Bingham, Voellmy and Quadratic rheology. Calibration was done on 1) the run-out distance, 2) the run-out time and 3) the goodness of fit with the thickness of the deposits along the track. In addition the erosion constant in the entrainment equation was calibrated on the observed versus calculated run-out volumes. Sensitivity analyses of the resistance parameters for the different rheologies showed that the viscosity, the basal friction, the turbulence term and the resistance factor are the most sensitive ones. It appeared that the variation in thickness along the run-out track can be explained by entrainment of material in the upper part of the track and a change in parametric values during the run-out process. The three rheologies produced a reasonable fit with the observed geometry of the run-out profile, run-out time and run-out volume. It was argued that the Voellmy rheology seems to give the most appropriate explanation for the difference in resistance along the run-out path. The main problem in the simulation was to stop the debris flow on a slope with a gradient around 22°.

A reactivation of the mass movement by frictional sliding of the material half way the run-out track was simulated. It occurred 30 min after the first run-out phase due to an increase in pore pressure. The sliding material changed into a slow flowing mass that reached a newly built up area after about 1 h and moved into Wangong Town over a distance of 80 m.

1. Introduction

This paper tries to explain the development of the Dagou mass movement, China, which started as a rock slide and changed into a rapid debris flow. A reactivation took place shortly after the first run-out phase: A part of the mass started again as a translational debris slide, which transformed into a slow moving flow.

There are a number of important issues related to the run-out of rapid mass movements like the initiation mechanisms, type of rheology controlling run-out processes, various entrainment and stopping mechanisms, and threat of reactivation, which happened with the Dagou mass movement. However, it is extremely difficult to determine in the field or laboratory reliable rheological values for these rapid mass movements. Some researchers tried to reconstruct the rheology and run-out mechanisms of debris flows by analysing the sedimentological and morphological characteristics of the deposits (e.g., Kelin et al., 1992; Whipple and Dunne, 1992; Imran et al., 2001; Iverson and Valance, 2001; Remaître et al., 2005a; Staley et al., 2006). In many cases numerical models are used for back calculation of the rheological parameters (e.g., Ayotte and Hungr, 2000; Chen and Lee, 2003; Bertolo and Wieczorek, 2005; Naef et al., 2006; Rickenmann et al., 2006; Medina et al., 2008; Begueria et al., 2009). These back analyses of debris flows are based on simplifications that attempt to reproduce the general features. In most cases calibration is based on constant rheological properties, which is good practise for a general assessment of future hazard and risk estimations in a certain region or locality. Many results of these back calculations from all over the world can be found in Quan Luna (2013). However there are few examples in literature, which try to reconstruct in more detail the transient character of the rheology, additional processes and reactivation of debris flows. One has to realize that the movement of these debris flows is complex and influenced by different additional processes such as various erosion processes along the track controlling velocity and run-out distances (McDougall and Hungr,

* Corresponding author. Tel.: +31 344 571449.
E-mail address: t.w.j.vanasch@uu.nl (T.W.J. van Asch).

http://dx.doi.org/10.1016/j.geomorph.2014.11.014
0169-555X/

2005; Remaître et al., 2005b; Chen et al., 2006; Quan Luna et al., 2012; Xu et al., 2012). Van Asch et al. (2004) drew attention to the use of the run-out profile of debris flows as an indicator of these changing run-out conditions. It is the aim of this paper to find out whether the run-out geometry of the Dagou mass movement can be used to reconstruct the transient character of these processes like changes in rheology and resistance parameters, entrainment, deposition and stopping. This will be done by means of 1D-numerical modelling and curve fitting on the run-out topography. In addition we will use the changes in the topographic profile to analyse the conditions of a reactivation, which occurred in this mass movement and which destroyed a part of Wangong Town. The back ground information for this study was obtained from a morphological analysis of this mass movement based on field investigations, eyewitness accounts and aerial photo interpretation (Xu et al., 2010).

2. Short description of the Dagou mass movement

The location of the study area in the Sichuan province of China is given in Fig. 1. The evolution of the so-called Dagou mass movement is described here briefly. More details can be found in Xu et al. (2010). The upper part of the Dagou catchment consists of basalts of the Ermeishan group (Pe) and the lower part of limestones of the Liangshan–Yangxing group (Pl + y), a Permian system, with a monoclonal structure. The superficial strata are strongly weathered and almost degraded into blocks. The dissolution of limestone created an uneven rock surface with a lot of karren. Quaternary debris flow deposits (Q4sef) and colluviums (Q4c + dl) are found at the mouth of the Dagou valley consisting of boulders, gravels, and silty clays, according to the Unified classification System (USCS).

Rainfall was the major triggering factor of the mass movement. From 23 to 25 July, two rainstorms hit the study area with a peak intensity of 6 and 50 mm h^{-1} respectively and a cumulative precipitation of 163 mm, which is 22% of the average yearly precipitation. In particular the rainfall on July 25 with an intensity of 50 mm h^{-1} and a return period of 50 years was fatal. The rainfall could penetrate into many vertical cracks in the source area and on 27 July, the mass movement started as a rock slide, which disintegrated quickly into debris.

Two consecutive run-out phases can be distinguished in the Dagou mass movement: a rapid rock slide/debris flow phase with a run-out distance of 1380 m and a run-out time of 50 s, and a reactivation phase characterised by a translational slide, which transformed into a slow moving flow. The whole secondary process lasted 4 h. Figs. 2 and 3 show the two phases in the run-out of the mass movement. The profiles of Fig. 3 were reconstructed in the field by means of topographical measurements and extrapolation of the original topography, measurements at the front of the mass movement, exposures due to excavation for rescue after the disaster, and exposures in the steep walls of the secondary gully, which developed in the second phase.

Xu et al. (2010) distinguished three zones in the first phase (Fig. 2): the source area (zone I), the transportation zone (zone II) and the deposition zone (zone III). Zone IV in Fig. 2 is the area, which was reactivated during the second run-out phase (see below). According to the local residents, a wide crack was generated on July 25 along the steep structural plane, before the occurrence of the mass movement on July 27. The crack finally formed the lateral boundary of the rockslide. At 4.40 AM on 27 July, several local residents heard a very loud sound combined with intensive ground shaking. The mass movement must have started as a rock slide and disintegrated into debris, moving down along the Dagou valley at a very high speed. The configuration and volume of the rock slide (480,000 m^3) could be determined in the field by two sets of joints forming respectively the head scarp and the sliding surface (Xu et al., 2010). The rock mass in the source area was densely jointed and strongly weathered and prone to degrade into a debris flow. The transportation zone II can be sub-divided into the main travelling channel (II-1) and the right and left bank entrainment zones (II-2 and II-3, respectively; Fig. 2). Here between 1500 and 1300 m asl., a significant amount of material was delivered to the flow from the plateau (zone II-2 (1)) and a valley side slope failure zone (zone II-2 (2)) of the left bank entrainment zone.

The grain size and weight of the sediments were measured in the field. A ruler was used to measure the grains with a size bigger than 100 mm, while the sieving method was adopted for the grains smaller than 100 mm.

Big boulders (USCS classification) were accumulated mainly in the upper part of the main travelling channel. The grain size of over 70% of the boulders is larger than 200 mm. Smaller grain sizes can be found in the lower part, which consisted of basalt fragments with soil. The grain size is evenly distributed over the different classes and 77% can be classified mainly as cobbles, and very coarse gravels (USCS classification) varying between 20 and 100 mm.

In the depositional zone III, the Dagou valley turns slightly to the right at about 1300 m asl., which led to a splitting of the debris into two branches (Fig. 2). Due to the inertial force, the left branch kept the original moving direction and climbed up to the left ridge. The right branch moved down along the Dagou valley concentrating most of the material into a channel with a width of around 50 m and a depth around 25 m. This channel ends at the exit of the valley and passes into the flat aforementioned Quaternary deposits. The thickness of the debris flow deposits increased from 5–10 m upstream to 15–25 m downstream. The grain size distribution of the right branch deposits shows that around 70% of the particles

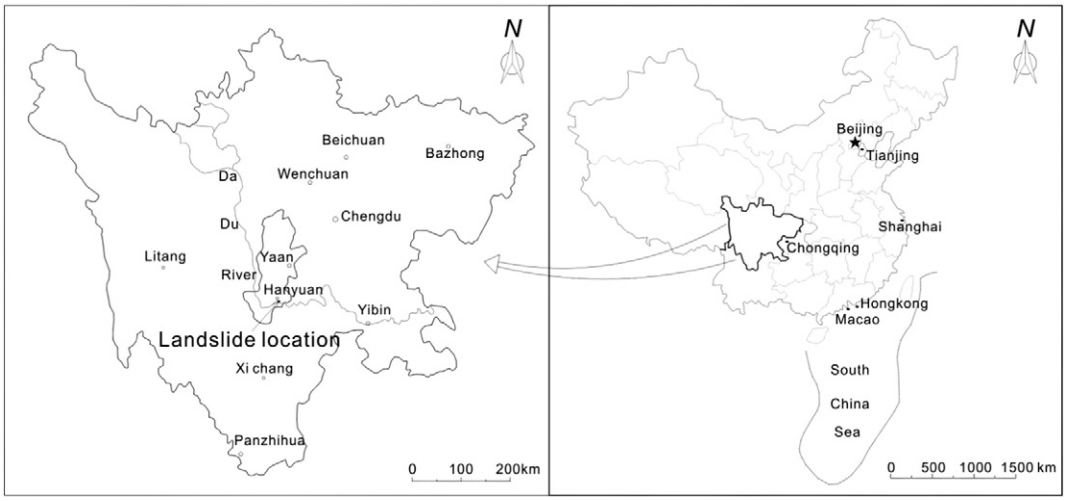

Fig. 1. Location of the study area in Sichuan province, China.

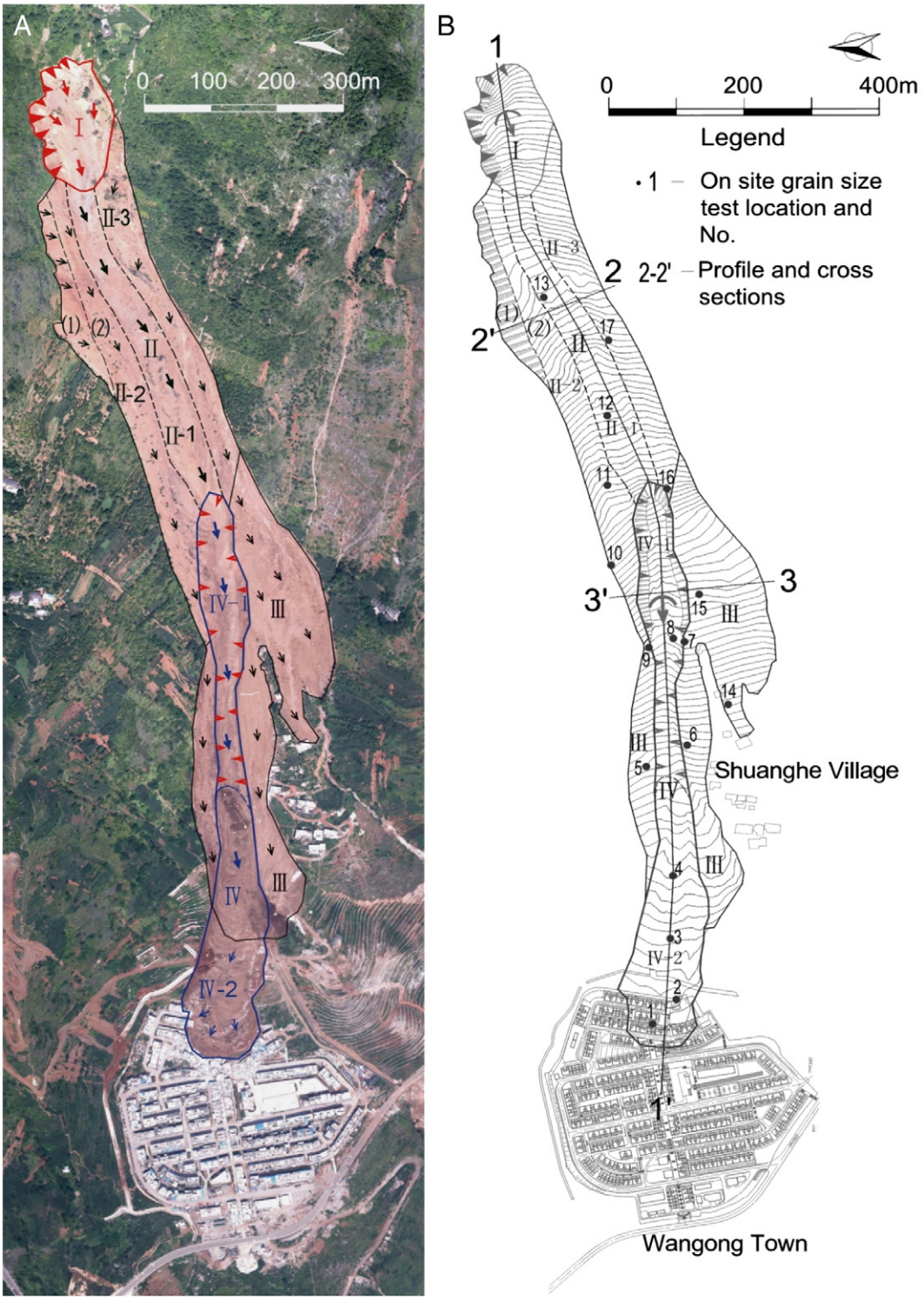

Fig. 2. Run-out of the Dagou landslide in two phases. A) Post-sliding aerial photo interpretation. B) Topographic map. Black arrows show the moving directions. See texts for the explanation of the zonation (after Xu et al., 2010, with kind permission of Springer Science + Business Media).

ranged from 10 to 100 mm in size (medium to coarse gravel and pebbles according to the USCS classification). The percentage of fines estimated in the field was around 25% with around 80% silt and 20% clay. A lot of splashed material on the back wall of a damaged house was observed indicating that the water content of the debris was very high.

After a half hour from the first run-out phase, the secondary movement started as a translational slide and transformed into a slow moving flow. The flow reached after about 1 h the newly built up area of Wangong Town at the foot of the slope. The front penetrated partly into the city over a distance of 80 m during 3 h, destroyed 92 homes, and forced the evacuation of 1500 people. The slow moving mass was obstructed by the buildings at the outskirts of Wangong Town.

Figs. 2 and 3B depict the head scarp and the area (zone IV-1) of the translational slide triggered in the second run-out phase (consisting of debris material deposited in the first run-out phase) and a deposition zone of the subsequent slow moving flow (zone IV-2). The debris

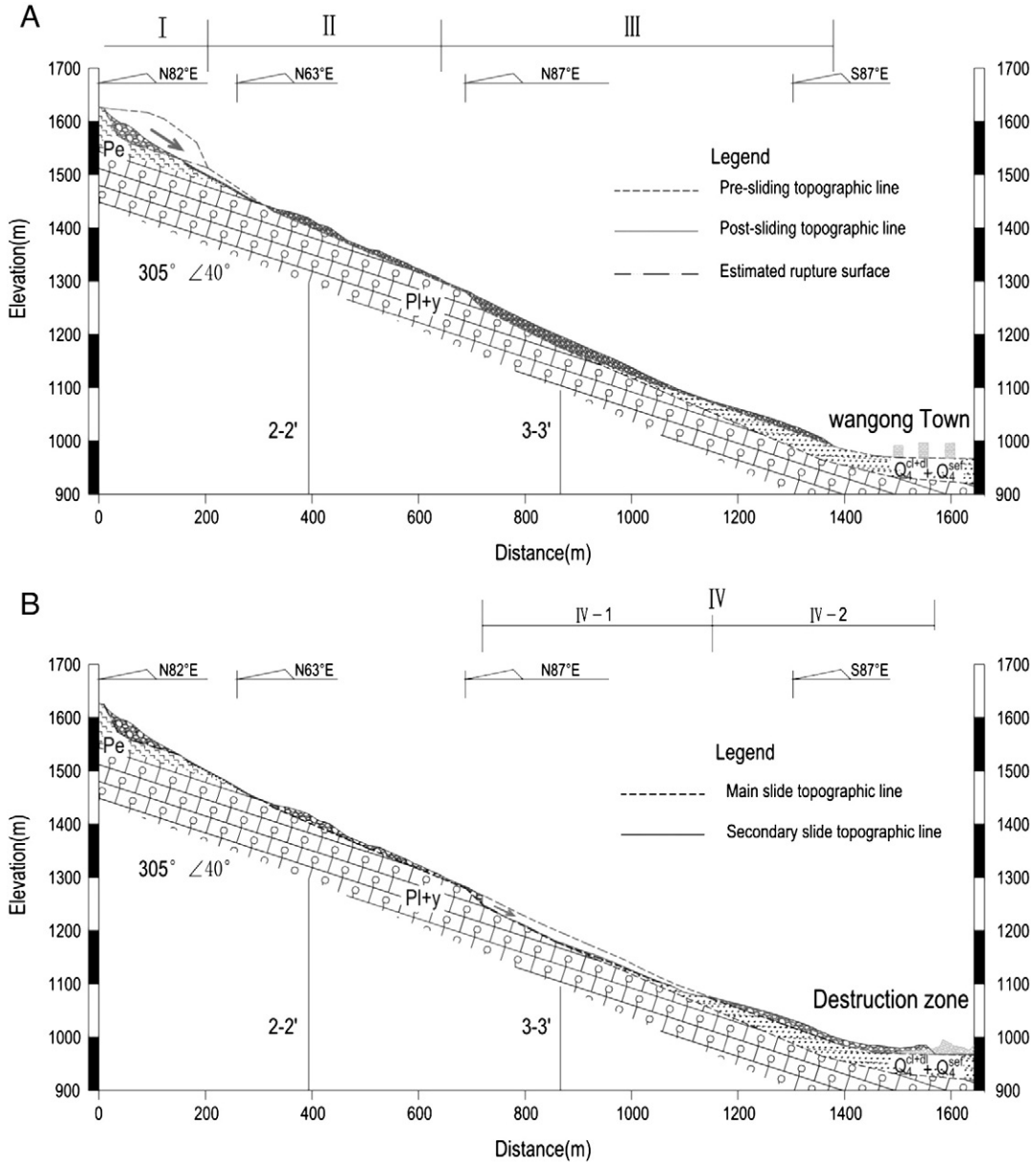

Fig. 3. Longitudinal geological profile along 1–1′ (Fig. 2B) and the run-out profiles with debris flow deposits. A) The first run-out phase; B) the second run-out phase (after Xu et al., 2010, with kind permission of Springer Science + Business Media).

material was nearly completely eroded over a length of 350 m (Fig. 3B). The average length and width of the deposition zone are 420 and 80 m respectively and shows lateral spreading. The width increases from about 35 to 110 m. The deposits are mainly composed of strongly weathered basalts. The materials in this zone have smaller grain sizes varying from 10 to 50 mm (medium to coarse gravel). The first main and second run-out movement have different mechanisms, which will be analysed more in detail in the next sections.

3. Model description

In order to analyse the run-out conditions of the Dagou mass movement, numerical model calculations were carried out to simulate some of the kinematic processes. For these simulations a classical approach was used based on the depth average shallow water equations. This has been applied by many authors (e.g., Hungr, 1995; Chen and Lee, 2003; Crosta et al., 2003; Mangeney et al., 2007; Medina et al., 2008; Begueria et al., 2009; Hungr and McDougall, 2009). The mass and momentum equations for a 1D simulation can be described as follows:

$$\frac{\partial h}{\partial t}+\frac{\partial (hu)}{\partial x}-\frac{\rho_s}{\rho}\frac{\partial d_{sc}}{\partial t}=0 \tag{1}$$

$$\frac{\partial u}{\partial t}+u\frac{\partial u}{\partial x}=g\left[\sin\alpha_x\cos\alpha_x-k\frac{\partial h}{\partial x}-S_f\right]-\frac{\rho_s}{\rho h}\frac{\partial (d_{sc}u)}{\partial t} \tag{2}$$

where h (m) is flow height, t (s) is time, u (m s^{-1}) is velocity, d_{sc} (m) is scouring depth, ρ and ρ_s (kg m^{-3}) are the mass density of flow and erodible soils respectively, and α_x (degrees) is the slope bed angle, which is taken positive when it dips downward in the (positive) x-direction. The momentum equation (Eq. (2)) is expressed in terms of acceleration (dimension LT^{-2}). The second term on the left side of Eq. (2) represents the convective acceleration. The first term on the right side of Eq. (2) represents the driving component with g, the acceleration due to gravity. The second term on the right side is the pressure

acceleration where k is the earth pressure coefficient (dimensionless), which ranges between two extreme values corresponding to the active and passive states in the Rankine theory (Savage and Hutter, 1989; Hungr, 1995). The third term on the right side, S_f, is the flow resistance due to frictional stress of the flowing mass with the bed. The fourth and last term on the right side of the equation expresses a loss in momentum due to the entrainment of material.

The resisting forces within the S_f term in Eq. (2) play an important role in the interpretation of deposition topography in this paper. It depends on the rheology of material, which controls the flow behaviour. Since there is not so much information about the geotechnical characteristics of material, three resistance terms (S_f) were used in our analyses for the first run-out of the debris flow phase of the mass movement. These three terms contain the most common resistance parameters used for different rheologies: the dominant viscous component (Bingham), the dominant frictional component (Voellmy) and a mixture of the two (Quadratic). The first one is the Coulomb–Viscous rheology or Bingham rheology when ϕ' (frictional resistance) is zero according to Coussot (1997):

$$S_f = \tan\varphi' + \frac{1}{\rho g h}\left(\frac{3}{2}\tau_c + \frac{3\eta}{h}u\right) \quad (3)$$

where τ_c (kPa) is yield strength, η (kPa s) is the viscosity parameter and $\tan\phi'$ is the apparent friction coefficient, which is controlled by the pore water pressure ratio:

$$\tan\varphi' = (1\text{-}r_u)\ \tan\varphi \quad (4)$$

with r_u as the internal pore water pressure ratio (the ratio between pore water pressure and total normal stress) and ϕ the intrinsic basal friction angle of flowing material.

The second term is the Voellmy resistance term (Voellmy, 1955):

$$S_f = \left[\tan\varphi' + \frac{u^2}{\xi h}\right] \equiv \left[\tan\varphi' + \frac{u^2}{C^2 h}\right] \quad (5)$$

where ξ (m s^{-2}) is the turbulence coefficient, which is similar to the square value of the Chézy resistance (C) for turbulent water flow.

The last resistance term incorporates a turbulent contribution to the yield strength and a viscous component (O'Brein et al., 1993):

$$S_f = \frac{\tau_c}{\rho g h} + \frac{K\eta}{8\rho g (h)^2}u + \frac{n^2(u)^2}{(h)^{4/3}} \quad (6)$$

where K is a resistance parameter that equals 24 for laminar flows in a smooth wide rectangular channel but increases with roughness and irregular cross sections; and n (m$^{-1/3}$ s) is the Manning coefficient that takes into account the turbulent and dispersive components of the flow.

Since entrainment was observed in the upper part of the travelling track, a simple erosion module has been included in our depth average model based on McDougal and Hungr (2005):

$$d_{sc} = E_r(hu)\,\Delta t \quad (7)$$

where E_r (m^{-1}) is an erosion constant, which we will use as a calibration factor.

The model was implemented in an explicit finite difference (Eulerian) mesh, i.e. the flow was described by a variation in the conservative variables at points of fixed coordinates (i) as a function of time (t). The mesh is defined as a regular grid. The equation is solved numerically using a central difference forward scheme. More details about the numerical implementation can be found in Begueria et al. (2009).

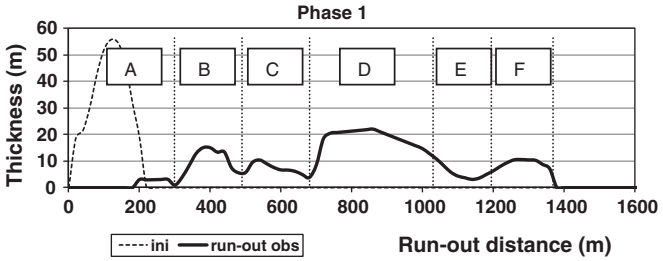

Fig. 4. Observed variation in thickness of the debris flow deposits along the track after the first run-out phase.

4. Analyses of the first run-out phase

4.1. Subdivision of the run-out geometry of the first phase

Fig. 4 shows, based on the profile given in Fig. 3A, the observed variation in the thickness of the deposits for the first run-out phase along the track. One can distinguish three distinct sections with a maximum thickness, namely sections B, D and F. B is the section with erosion, and thus with an external input of material. Section D shows a clear sediment accumulation in the channel. It remains to be seen whether a change in rheology, especially an increase in resistance S_f has contributed to the accumulation of material. Section E is the accumulation area of the in situ Quaternary debris flow deposits (Q4sef) and colluviums (Q4c + dl), which is not dissected by a channel. The Dagou flow material, leaving the channel in section D, could spread evenly over the flat area, which causes a decrease in thickness in our observed profile. Further down slope in section F, the effect of a decrease in slope gradient and increase in friction on this ancient material may have caused an increase in accumulation (Figs. 3A and 4).

4.2. Model calibration and parameterization

The variation in thickness is controlled by changes in resistance, entrainment of material as observed in the upper part of the run-out track (Xu et al., 2010) and topographical effects of the original ground surface. As was mentioned already, the resistance for the three rheologies is described by the S_f term, which consists of different resistance parameters (Eqs. (3)–(6)). The entrainment effect is expressed by the last term of Eq. (2) and by Eq. (7).

The change in thickness along the profile is also influenced by the fact that half way the run-out track the open slope changes into a channelled slope. The corrected thickness h_c (m) due to confinement and accumulation into this channel can be approximated as follows:

$$h_c = h_2 + \frac{h_1 B_1 - {}^1\!/_2 h_2 B_2}{B_1} \quad (8)$$

where h_1 is the initial thickness of the debris flow on a flat slope; B_1 is the initial width of the debris flow on a flat plane; h_2 is the incision depth of the gully into the flat plane and B_2 is the maximum width of the gully with a triangular cross section in our case.

Calibration was done by fitting the values of the resistance parameters and the gully parameters on 1) run-out distance (*ROD*), 2) run-out time (*ROT*) and 3) goodness of fit with the thickness of the deposits along the track (Table 1). The goodness of topographical fit was tested using the normalized root mean square error (*NRMS*) (%):

$$NRMS = \frac{\sqrt{\frac{1}{m}\sum_{i=1}^{i=m}\left(h_{calc,i} - h_{obs,i}\right)^2}}{h_{max} - h_{min}} 100\% \quad (9)$$

Table 1
Calibrated parametric values for zones B to F. *ROD* is run-out distance; *ROT* run-out time; *OV/CV* observed/calculated run-out volume to calibrate the erosion factor; *NMRS* is normalized mean root square. For explanation of the rheologic parameters see text.

Rheology	Parameter	Sect. B	Sect. C	Sect. D	Gully geometry. (m) in D	Sect. E	Sect F	*ROD* 1380 m	*ROT* 50 s	*OV/CV* 1.00	*NMRS* 0%
Bingham	τ_0 (kPa)	5	1	1	$B_1 = 170$	1	5	1420	43.50	1.02	10.58
	η (kPa s)	120	2	*120*	$B_2 = 50$	2	120				
	E_r	0.016	0.0	0.0	$h_2 = 30$	0.0	0.0				
Voellmy	f (−)	0.267	0.18	0.18	$B_1 = 150$	0.18	0.267	1400	41.30	1.11	13.83
	C	1.2	10	10	$B_2 = 50$	10	0.4				
	E_r	0.006	0.0	0.0	$h_2 = 25$ m	0.0	0.0				
Quadratic	τ_0 (kPa)	1	1	1	$B_1 = 130$	1	10	1380	40.83	1.03	11.94
	η (kPa s)	180	12	12	$B_2 = 70$	12	300				
	K	25	25	70	$h_2 = 25$ m	25	25				
	n	0.04	0.04	0.04		0.04	0.04				
	E_r	0.028	0.0	0.0		0.0	0.0				

where m is the total number of calculation nodes along the track; $h_{calc,\,i}$ and $h_{obs,\,i}$ are the calculated and observed thicknesses at node i, respectively, and h_{max} and h_{min} the maximum and minimum observed thicknesses along the track, respectively. In addition we calibrated the erosion parameter E_r (Eq. (7)) on the observed versus calculated run-out volumes per metre width (*OV/CV*, Table 1) assuming no effect on the cross sectional height by the channel.

Table 1 shows the calibrated values for the various parameters for each section, and the values for the four calibration criteria (*ROD*, *ROT*, *OV/CV*, and *NMRS*) in the last four columns. The ideal scoring values are indicated at the head of these columns.

Fig. 5 gives the calculated run-out topography compared to the observed run-out topography. The figure and Table 1 (*NMRS*) show that a reasonable fit can be obtained with the observed topographic surface of the deposits assuming erosion and differences in resistance along the track as expressed by the parameters in Table 1 and including the topographic effect of the gully in section D. In our simulations the run-out time is a bit shorter than what was reported by eyewitnesses.

4.3. Sensitivity analyses

Following Remaître et al. (2008) and Quan Luna et al. (2012), a sensitivity analysis was performed to find out which are the most important resistance parameters influencing the deposition geometry. Therefore the maximum and minimum values of the calibrated parameters given in Table 1 were stepwise increased and decreased with a certain percentage until 100% of the values given in Table 1. Fig. 6 gives the results, showing the effect of the percentage deviation from the calibrated parametric values (x-axis) to the *NRMS* of the calculated deposition topography (y-axis). The most sensitive parameter in the Bingham rheology proved to be the viscosity (Fig. 6A) while the yield strength has nearly no effect on the topographic distribution of the

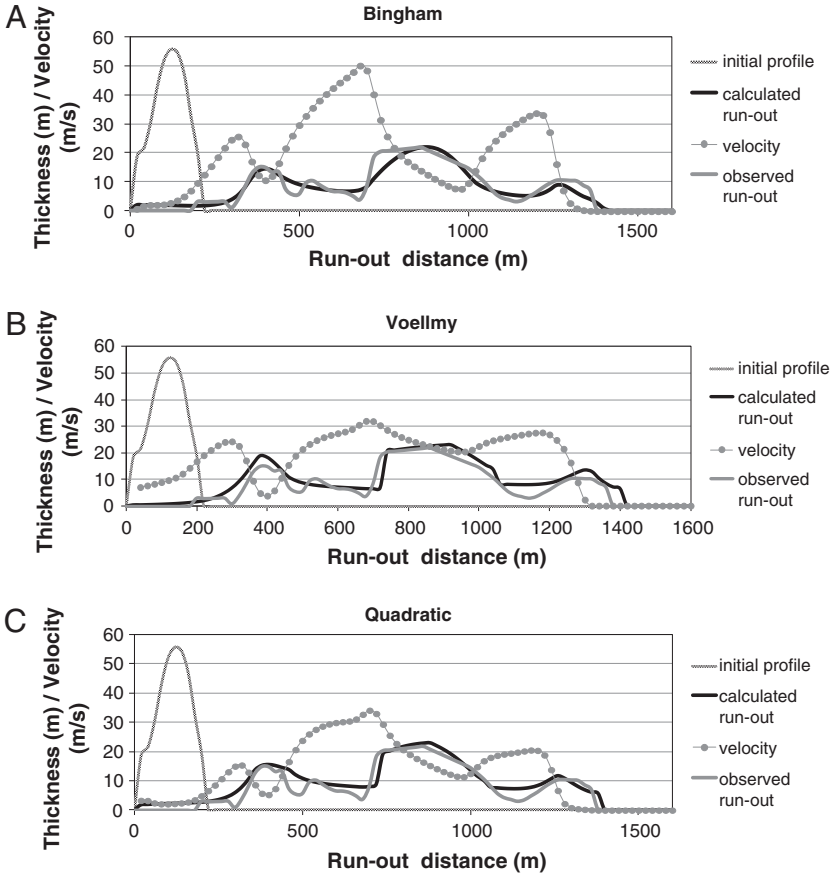

Fig. 5. Calculated versus observed run-out profiles and the end velocities after the first run-out phase for the three rheologies: A) Bingham, B) Voellmy and C) Quadratic.

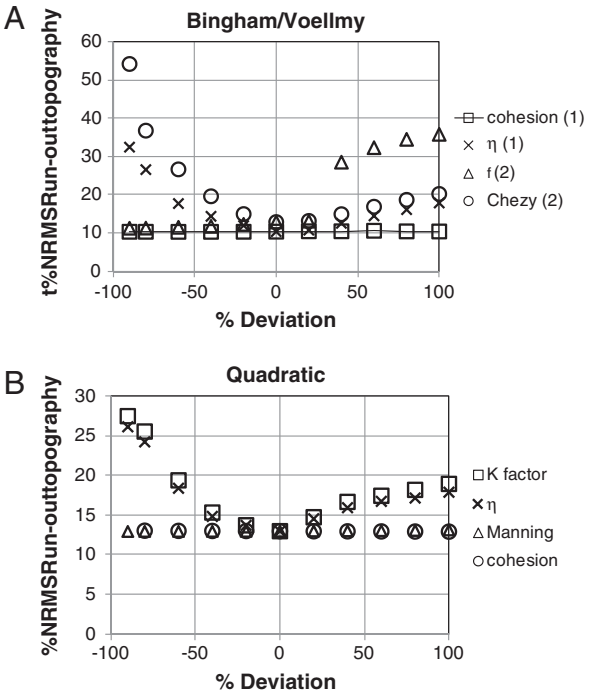

Fig. 6. Sensitivity of the S_t-resistance parameters for the three rheologies: A) Bingham/Voellmy and B) Quadratic.

run-out mass. For the Voellmy rheology the basal friction $f\,(=\tan\phi')$ and the Chézy factor C have a large effect on the variation in thickness. Fig. 6B shows that for the Quadratic rheology the K factor and the viscosity are the most effective parameters determining the differences in topographic height of the run-out mass.

4.4. Reduction of velocity

Fig. 5 shows the distribution of the velocity along the run-out track after 40 s. It is shown that at that time the speed of the debris flow along some parts of the track is still rather high. Only the front velocity has reduced to zero. In order to reduce the speed at some places along the track, one can gradually increase the resistance of the most sensitive parameters during the run-out. These are the viscosity, the basal friction and the Chezy turbulence factor according to Section 4.3. An attempt to introduce a gradual increase of these resistance parameters, to mimic during the run-out pore pressure dissipation or loss of water, produced a poor match with the observed deposition geometry. Increase of the resistance of the flow must have occurred during the last phase of the run-out process. Table 1 shows that the run-out time to reach the run-out topography shown in Fig. 5 for the three rheologies is around 40 s. We prolonged the run-out simulation with 10 s until the observed run-out time of 50 s. During this prolongation we increased the resistance parameters (viscosity, basal friction and the Chezy turbulence factor). Fig. 7 shows the velocity distribution along the run-out track at the run-out time of 40 s for the three rheologies like in Fig. 5. Also is shown the velocity distribution after 50 s. No movement can be seen anymore at the front between the time of 40 and 50 s but a drastic reduction in the velocity at some places along the run-out track.

4.5. Interpretation of the modelling results of run-out phase 1

We explain here how the resistance parameters, erosion and underground topography have influenced the thickness of run-out material in the different sections. Section A is the source area with a change from a slide into a debris flow. We did not model this transformation process. Section B is an area where significant erosion could be detected (Xu et al., 2010; see also Sections 2 and 4.1). The external input in this section of material by erosion and landslip failure of the side walls has contributed to the relative increase in thickness of the deposit. The erosion term in Eq. (2) causes a loss of momentum and velocity which contributes to the increase in thickness. Also the large concentration of boulders found here must have increased the friction (see Section 2). These phenomena were simulated with a change in section B of the most sensitive parameters in the Voellmy rheology (Fig. 5A): an increase of the basal friction term f and a decrease of the Chézy factor (C) (Table 1). In the case of a Bingham or Quadratic rheology, we increased the viscosity parameter (Fig. 5A,B and Table 1), which may simulate the input of drier eroded material (Table 1).

Section D shows again a clear accumulation of the material (Figs. 3 and 4). In this section the material in the left branch concentrates into a distinct channel (see Section 2) about 50 m in width and 30 m in depth (dimensions based on a cross section give by Xu et al., 2010). In the case of a Voellmy rheology the increase in thickness could be simulated rather well based only on a correction for the channel topography (Eq. (8); Fig. 5B and Table 1) For the Quadratic rheology a combination of an increase of the K factor and the topographical correction delivered also good results (Fig. 5C and Table 1). An increase of the K factor seems logical because the flow transformed from a wide unconfined flow to a concentrated channel flow. With respect to the Bigham rheology the best fitting results could only be obtained by an increase of the viscosity in combination with the topographic correction (Table 1).

The decrease in material thickness in section E is associated with the transition from the channel to the flat deposition surface of the Quaternary sediments. This was simulated by a gradual reduction of the depth of the channel. Section F shows again an increased thickness of debris, which is caused by a decrease of slope gradient. But the decrease in

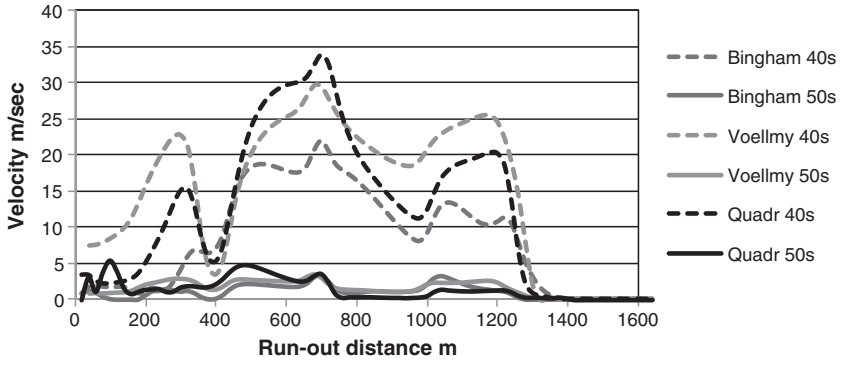

Fig. 7. Decrease in the velocity distribution along the track from the calculated run-out time around 40 s (Table 1) until the observed run-out time of 50 s, by a gradual increase of the viscosity to an end value of 200 and 600 kPa for the Bingham and Quadratic options respectively. For the Voellmy rheology an increase in the friction factor until $\phi' = 21°$ and a decrease in the Chézy factor until 2.

slope gradient was not enough to simulate the accumulation of material in section F. There must have been also an effect of the underlying loose material (Fig. 3). Iverson et al. (2011) described the effect of in situ loose material on the run-out of debris flows. They showed that in very wet sediments pore pressure increases and friction decreases while there is an opposite effect in case of drier sediments. Then the flow momentum and velocity decrease, while friction increases due to dissipation of pore pressure. Therefore in order to get a good topographical fit in section F we increased the most sensitive resistance parameters (Table 1), which implies that the underlying Quaternary sediments were relatively dry. It is also possible that the increase in friction and (or) viscosity might be explained by a pushing down of debris flow material into the apparently weaker Quaternary deposits or by partial entrainment of those deposits. No evidence of entrained material (like in section B) was found in the field but that could be masked by the secondary slow movement of debris into the city.

As we have seen, reasonable simulation results can be obtained along the track with the three rheologies. The question arises whether in all cases a physical explanation can be given for the change in rheological characteristics. In section B we increased the friction (Voellmy) and the viscosity (Bingham and Quadratic; Table 1) which can be explained by the input of drier material and decrease in momentum. It is more difficult to explain why in the Bingham simulation the viscosity should increase in the channel of section D as was required for the calibration. For the quadratic rheology we had to increase the K factor in the channel of section D, which seems reasonable because the flow became more confined. It is also difficult to explain for the Quadratic and Bingham scenarios why the viscosity has to increase so dramatically in section F. It is most likely that the first (main) run-out phase was controlled by a Voellmy rheology because in section B the erosion and input of material into the flow can be explained by an increase in friction and a lower turbidity. In section D no change in rheology was needed (Table 1) but only a correction of the flow thickness (Eq. (8)) due to inflow into the channel, while in section F the increase in friction is caused by increase in apparent friction through the loss of pore pressure caused by pore pressure dissipation through the drier underlying Quaternary material.

5. Analysis of the second run-out phase

The second run-out profile shows a nearly complete removal of debris flow material between 700 and 1100 m deposited in the first phase, (Figs. 3 and 8, zone IV-1). Zone IV-2 lies between 1175 and 1580 m where the material was moving slowly (see Section 2). The following reconstruction can be made for the reactivation process: the material was deposited in the gully during the first run-out as a frictional material. We simulated with a Voellmy rheology, during most of the run-out time an effective basic friction angle of $f = 0.18$ which means an apparent (effective) ϕ' of 10.2° (Table 1 and Eq. (3)). Since the mean slope inclination along the middle part of the trajectory is around 20°, the apparent friction angle must have increased by dissipation of excess pore pressure and partial drainage to reach at least an apparent friction around $\phi' = 21°$ in order to arrive at a meta-stable condition. The material in this section (zone IV-1) was reactivated according to Xu et al. (2010) after half an hour. This must have happened by a slight rise of the groundwater supplied by a source, which was observed before the mass movement at the head of the gully, which coincides with the scarp of the reactivated mass movement (X. Zhou, personal communication). We reactivated the mass movement in our simulation in zone IV-1 as a frictional slide, with an effective friction angle of 18.5° and a zero cohesion (pure frictional rheology; $S_f = \tan\phi'$, Table 2) Because the mass had no cohesion it could fail over its total depth. In zone IV-2 we assumed a Bingham behaviour in the pathway to Wangong Town with a relative high viscosity of 8.5E + 05 kPa s. To mimic friction exerted by the buildings in the urban area, a quasi frictional component was added ($\phi = 16°$) to the viscosity (Table 2). According to our modelling, the toe of the landslide in zone IV-2 arrived at the border of Wangong Town at 1500 m after 70 min according to eyewitnesses after about one hour (Table 2). According to our calculations it slowly moved into the town and stopped after 60 m (80 m observed) and 255 min after the initiation (about 4 h; Table 2).

During the 1D run-out simulation a factor was introduced, which took into account the spreading in the fan-shaped accumulation zone (zone IV in Fig. 2; see Section 2). This fan shape can be described as a trapezium with a width at the top and bottom of 32 and 116 m respectively and a longitudinal length of 240 m. The correction for the thickness in the profile due to spreading of the debris can be described as follows:

$$\Delta h_c = \frac{\Delta h(w_t \tan\beta + 2x)}{(w_t \tan\beta + 2x + \Delta x)} \quad (10)$$

where Δh_c is the corrected change in thickness at a distance x from the top of the fan shape (trapezium) over a finite distance Δx; Δh is the change in thickness over Δx, in case of no spreading, w_t is the width at the top and β is the angle of the legs of the trapezium shape of the fan. In this way the same calculated and observed volume per metre width ($OV/CV = 1$) was obtained, and a reasonable good fit with the topography ($NMRS = 12.71\%$ (Table 2)

Fig. 8 shows that we could not simulate the two observed maxima and the depression of the landslide deposit, which may be a relic of the initial topography of the first run-out phase.

6. Discussion and conclusions

This paper reconstructed the run-out conditions of a multi phase mass movement by means of a fitting procedure on a deposition profile using different rheologies. Since the previous study of this mass movement had not reported detailed information about the hydro-mechanical characteristics of the material, three rheologies were used, ranging from viscous to frictional. It appeared that calibration by changing the resistance parameters for each rheology gave reasonable fits with the observed deposition topography, run-out time and distance.

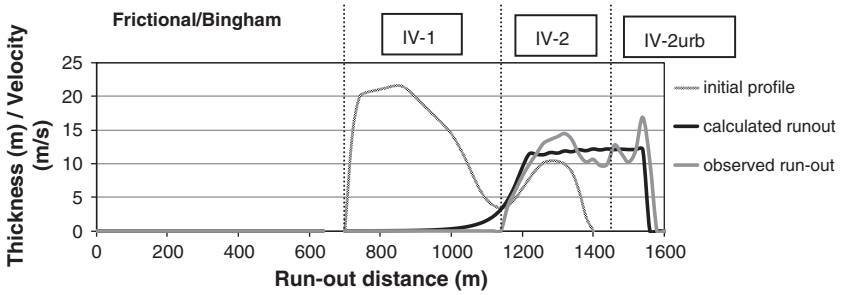

Fig. 8. Calculated versus observed run-out profiles for the second run-out phase in zones IV-1, IV-2 and IV-2-urb (urban area) with a transformation from a Frictional, Bingham and quasi-Coulomb viscous rheology respectively.

Table 2
Calibrated parametric values for zones IV-1 and IV-2 (see Fig. 8). *ROT* run-out time to the border of the city at 1500 m and the final run-out time; *ROD* is the final run-outdistance; *OV/CV* observed /calculated run-out volume; *NMRS* is normalized mean root square error. The rheological parameter symbols are explained in Eqs. (3) to (8). Target figures for the calibration in italics at the head of the last five columns.

	IV-I	IV-2	IV-2_{urb}	*ROT* border ± 60 min	*ROT* final ± 240 min	*ROD* final 1580 m	*OV/CV* 1.0	*NMRS* 0%
ϕ' (–)	18.5°			51 min	256 min	1560 m	1.0	12.71%
ϕ building			16^0					
η (kPa s)	0	8.5E + 05	8.5E + 05					
c (kPa)	0	2	2					

Therefore the run-out profile of the mass movement was not discriminatory for the three rheologies. However we were able to show that change in the values of the governing resistance parameters within these rheologies and other factors affects the run-out geometry.

The most sensitive resistance parameters appeared to be the viscosity in the Bingham and Quadratic rheology and the friction and the Chezy factor in the Voellmy rheology. Nevertheless the change of these sensitive parameters to fit the observed deposition geometry is sometimes difficult to explain physically. It is not easy to understand for example why in the Bingham simulation the viscosity should increase in the channel of section D. Also, did the Quaternary material on the lower slope gradient in section F increase the viscosity?

Despite a lesser fit with the observed deposition geometry, the Voellmy rheology seems to give the most suitable explanation for the difference in resistance along the run-out path. The second run-out phase could be simulated as a classic slide-flow complex where in the source area a pure frictional plastic failure was assumed and in the deposition area a Bingham rheology and for the built-up area a quasi Coulomb-Viscous rheology respectively.

We were able, up to a certain level, to unravel the circumstances, which explain the run-out profile of a complex mass movement and its reactivation but it certainly have raised questions. The biggest problem was that despite the reasonable fit we could make with the run-out profile, time and distance, we were not able to stabilize most of the debris material on such a steep slope with an average gradient of 20°. To stop the debris flow in the first run-out phase, we have to assume a rapid increase in friction in a short time induced by pore pressure dissipation and/or loss of water to increase the basal friction or the viscosity. Even if we were able to get reasonable fits assuming a more gradual dissipation over the total run-out time of 50 s, there exist doubts about the possibility of pore pressure dissipation during moving of the flow (e.g., Major, 2000). Major and Iverson (1999) postulated that leading edges of debris flows exhibit little or no positive pore-fluid pressure. Deposition therefore resulted from higher frictional strength concentrated at the flow margins. But it is hard to believe that the higher strength of the material at the border of such a steep channel in section D could stop the flow with a thickness of 20 m. Also the concentration of the coarsest rock fragments along the edges of the debris flow during run-out can increase the marginal strength. However such concentrations of rock fragments along the sides were not observed in the field. A possible increase of fines in section D estimated at about 25% may increase the yield strength of the mass but in our view it is not enough to stop a debris flow with such a steep gradient with a thickness around 20 m.

To improve our run-out models we must continue to focus on important features such as flow regime transitions, entrainment and stopping mechanisms. Detailed back analyses of well documented events and also focusing on the topographic characteristics of the debris flow deposits will be useful in understanding the dynamics of these processes.

Acknowledgement

We thank the two anonymous reviewers for their valuable comments and suggestions, which improved our paper.

References

Ayotte, D., Hungr, O., 2000. Calibration of a Run-out Prediction Model for Debris Flows and Avalanches. In: Wieczorek, G.F., Naeser, N.D. (Eds.), Debris flow Hazard Mitigation: Mechanics Prediction and Assessment. Proceedings of the Second International Conference on Debris flow Hazard Mitigation, Taipei, (Taiwan). Balkema, Rotterdam, pp. 505–514.
Begueria, S., Van Asch, Th.W.J., Malet, J.-P., Grondahl, S., 2009. A GIS-based numerical model for simulating the kinematics of mud and debris flows over complex terrain. Nat. Hazards Earth Syst. Sci. 9, 1897–1909.
Bertolo, P., Wieczorek, G.F., 2005. Calibration of numerical models for small debris flows in Yosemite Valley, California, USA. Nat. Hazards Earth Syst. Sci. 5, 993–1001.
Chen, H., Lee, C.F., 2003. Numerical simulation of debris flows. Can. Geotech. J. 37, 146–160.
Chen, H., Crosta, G.B., Lee, C.F., 2006. Erosional effects on run-out of fast landslides debris flows and avalanches: a numerical investigation. Geotechnique 56, 305–322.
Coussot, P., 1997. Mudflow Rheology and Dynamics. Balkema, Rotterdam.
Crosta, G.B., Imposimato, S., Roddeman, D., 2003. Numerical modelling of large landslides stability and run-out. Nat. Hazards Earth Syst. Sci. 3, 523–538.
Hungr, O., 1995. A model for the run-out analysis of rapid flow slides, debris flows and avalanches. Can. Geotech. J. 32, 610–623.
Hungr, O., McDougall, S., 2009. Two numerical models for landslide dynamic analysis. Comput. Geosci. 35, 978–992.
Imran, J., Parker, G., Locat, J., Lee, H., 2001. 1D numerical model of muddy subaqueous and sub-aerial debris flows. J. Hydraul. Eng. 127, 959–968.
Iverson, M.I., Vallance, J.W., 2001. New views on granular flows. Geology 29, 115–118.
Iverson, R.M., Reid, M.E., Logan, M., LaHusen, R.G., Godt, J.W., Griswold, J.P., 2011. Positive feedback and momentum growth during debris flow entrainment of wet bed sediment. Nat. Geosci. 4, 116–121.
Kelin, X., Whipple, X., Dunne, T., 1992. The influence of debris-flow rheology on fan morphology, Owens Valley, California. Bulletin of the Geological Society of America 104 (7), 887–900.
Major, J.J., 2000. Gravity-driven consolidation of granular slurries: implications for debris flow deposition and deposit characteristics. J. Sediment. Res. 70, 64–83.
Major, J.J., Iverson, R.M., 1999. Debris-flow deposition: effects of pore-fluid pressure and friction concentrated at flow margins. Bull. Geol. Soc. Am. 111, 1424–1434.
Mangeney, A., Tsimring, L.S., Volfson, D., Aranson, I.S., Bouchut, F., 2007. Avalanche mobility induced by the presence of an erodible bed and associated entrainment. Geophys. Res. Lett. 34, L22401. http://dx.doi.org/10.1029/2007GL031348.
McDougal, S., Hungr, O., 2005. Dynamic modelling of entrainment in rapid landslides. Can. Geotech. J. 42, 1437–1448.
Medina, V., Hürlimann, M., Bateman, A., 2008. Application of FLATModel, a 2D finite volume code, to debris flows in the north-eastern part of the Iberian Peninsula. Landslides 5, 127–142.
Naef, D., Rickenmann, D., Rutchmann, P., Mc Ardell, B.W., 2006. Comparison of flow resistance relations for debris flows using a one-dimensional finite element simulation model. Nat. Hazards Earth Syst. Sci. 6, 155–165.
O' Brien, J.S., Julien, P.Y., Fullerton, W.T., 1993. Two dimensional water flood and mudflow simulation. J. Hydraul. Eng. 119, 244–261.
Quan Luna, B., 2013. Dynamic numerical run-out modelling for quantitative landslide risk assessment. ITC dissertation no 206. Thesis University of Twente ((238 pp). http://www.itc.nl/library/papers_2012/phd/quan.pdf.).
Quan Luna, B., Remaître, A., Van Asch, Th.W.J., Malet, J.P., Van Westen, C.J., 2012. Analysis of debris flow behaviour with a one dimensional run-out model incorporating entrainment. Eng. Geol. 128, 63–75.
Remaître, A., Maquaire, O., Malet, J.-P., 2005a. Morphology and sedimentology of a complex debris flow in clay-shales basins. Earth Surf. Process. Landf. 30, 339–348.
Remaître, A., Malet, J.-P., Maquaire, O., Ancey, C., Locat, J., 2005b. Flow behaviour and run-out modelling of a complex debris flow in a clay-shale basin. Earth Surf. Process. Landf. 30, 479–488.
Remaître, A., van Asch, Th.W.J., Malet, J.-P., Maquaire, O., 2008. Influence of check dams on debris flow run-out intensity. Nat. Hazards Earth Syst. Sci. 8, 1403–1416.
Rickenmann, D., Laigle, B., McArdell, B.W., Hűbl, J., 2006. Comparison of 2D debris flow simulation models with field events. Comput. Geosci. 10, 241–264.
Savage, S.B., Hutter, K., 1989. The motion of a finite mass of granular material down a rough incline. J. Fluid Mech. 199, 177–215.
Staley, D.M., Wasklewicz, T.A., Blaszczynski, J.S., 2006. Surficial patterns of debris flow deposition on alluvial fans in Death Valley, CA using airborne laser swath mapping data. Geomorphology 74, 152–163.

van Asch, Th.W.J., Malet, J.-P., Remaître, A., Maquaire, O., 2004. Numerical modelling of the run-out of a muddy debris flow. The effect of rheology on velocity and deposit thickness along the run-out track. In: Lacerda, W. (Ed.), Proceedings of the 9th International Symposium on landslides, Rio de Janeiro, Brasil 1. Balkema, Rotterdam, pp. 1433–1438.

Voellmy, A., 1955. Über die Zerstőrungskraft von Lawinen. Schweiz. Bauzeitung 7, 212–285.

Whipple, K.X., Dunne, Th., 1992. The influence of debris-flow rheology on fan morphology, Owens Valley, California. Bull. Geol. Soc. Am. 104, 887–900.

Xu, Q., Fan, X., Dong, X., 2010. Characteristics and formation mechanism of a catastrophic rainfall-induced rock avalanche-mud flow in Sichuan, China. Landslides 9, 143–154.

Xu, Q., Shang, Y., Van Asch, Th.W.J., Wang, S., Zhang, Z., Dong, X., 2012. Observations from the large, rapid Yigong rockslide-debris avalanche, southeast Tibet. Can. Geotech. J. 49, 589–606.